JOURNAL OF SPACECRAFT AND ROCKETS
Vol. 39, No. 6, November–December 2002

Plume Modeling of Stationary Plasma Thrusters and Interactions with the Express-A Spacecraft

Ioannis G. Mikellides* and Gary A. Jongeward†
Science Applications International Corporation, San Diego, California 92121
Ira Katz‡
Jet Propulsion Laboratory, California Institute of Technology, Pasadena, California 91109
and
David H. Manzella§
University of Toledo, Toledo, Ohio 43606

Hall-effect thruster flight measurements are compared with results from two-dimensional plume and three-dimensional spacecraft interactions computer simulations. The measurements were acquired onboard Express-A 2 and A 3, two Russian communications satellites in geosynchronus orbit. The spacecraft carry four propulsion units for east–west and north–south station keeping. Each unit consists of two stationary plasma thrusters. Ion flux and energy spectra were recorded at various positions with respect to the thrusters and are compared with results from simulations using a uniform electron temperature, two-dimensional plume code that computes the expansion of the main ion beam by a fluid approach. The dynamics of the charge-exchange plasma are determined by a particle-in-cell method. Comparisons suggest good agreement for plume angles less than 40 deg and electron temperature between 8 and 11 eV. At approximately 4 and 9 m away from the thruster, and at plume angles less than 10 deg, the discrepancy between measured and computed values is found to be less than 10%. At larger angles, ion flux measurements exhibit large variations during operation of the same thruster. At 80 deg and 1.35 m away from the thruster, flux sensors recorded current densities that ranged between 12 and 55 mA/m^2. The two-dimensional code computes 27 mA/m^2 for an anode mass flow rate of 5.3 mg/s at this location. Moments induced on the spacecraft during the operation of each thruster were also recorded by the attitude control system and are compared with results from a three-dimensional spacecraft interactions code. These measurements were taken during rotation of the solar arrays.

Nomenclature

$\boldsymbol{a}$	=	acceleration vector of an ion mass element, m/s^2
$\mathrm{d}\boldsymbol{f}$	=	incremental force on a surface element, N
$\boldsymbol{E}$	=	electric field, V/m
e	=	electron charge, C
$F_{A,\mathrm{HET}}$	=	anode flow rate, kg/s
F_0	=	flow rate of neutrals from a cylinder, kg/s
$F_{0,\mathrm{HC}}$	=	flow rate of neutrals from the hollow cathode, kg/s
$F_{0,\mathrm{HET}}$	=	flow rate of neutrals from the Hall-effect thruster (HET), kg/s
$\boldsymbol{f}_d$	=	force on a fully diffuse surface due to incident plume particles, N
$\boldsymbol{f}_j$	=	momentum imparted onto a surface j from plume particles, per unit time, N
$\boldsymbol{f}_s$	=	force on a specular surface due to incident plume particles, N
$\boldsymbol{f}_T$	=	thrust vector, N
m_e	=	electron mass, kg
m_i	=	ion mass, kg
$\boldsymbol{n}$	=	plasma density, m^{-3}
$\boldsymbol{n}$	=	unit vector normal to surface
n_0	=	total particle density of neutrals, m^{-3}
$n_{0,\mathrm{cyl}}$	=	particle density of neutrals from a cylinder, m^{-3}
$n_{0,\mathrm{HC}}$	=	particle density of neutrals from the hollow cathode, m^{-3}
$n_{0,\mathrm{HET}}$	=	particle density of neutrals from the HET, m^{-3}
n_∞	=	(reference) plasma density at zero potential, m^{-3}
$\dot{n}_{\mathrm{CEX}}$	=	ion production rate from charge exchange, 1/m$^3 \cdot$ s
p	=	electron pressure, Pa
$\boldsymbol{r}$	=	position vector of an ion mass element, m
r_{HC}	=	distance of hollow cathode from the centerline, m
$\boldsymbol{r}_0$	=	initial position vector of an ion mass element, m
T_e	=	electron temperature, eV
t	=	time, s
$\boldsymbol{u}_{\mathrm{inc}}$	=	velocity of particles incident to a surface, m/s
$u_{i,\mathrm{exit}}$	=	ion speed at the thruster exit, m/s
$\boldsymbol{u}_{\mathrm{ref}}$	=	velocity of reflected particles from a surface, m/s
u_0	=	speed of neutrals at the exit of a cylindrical channel, m/s
$u_{0,\mathrm{HC}}$	=	speed of neutrals at the exit of the hollow cathode, m/s
$u_{0,\mathrm{HET}}$	=	speed of neutrals at the HET exit, m/s
$\boldsymbol{V}$	=	ion drift velocity, m/s
$\boldsymbol{V}_0$	=	initial ion drift velocity, m/s
$\boldsymbol{v}_e$	=	electron thermal velocity, m/s
$\boldsymbol{\Gamma}$	=	torque, m $\cdot$ N
$\Delta\boldsymbol{R}_j$	=	position vector of a surface j from a reference point, m
$\Delta\boldsymbol{R}_T$	=	position vector of a thruster from a reference point, m
ρ	=	radius of a cylinder, m
ρ_{in}	=	inner radius of the HET acceleration channel, m
ρ_{out}	=	outer radius of the HET acceleration channel, m
σ_{CEX}	=	resonant charge-exchange collision cross section, m^2
ϕ	=	electric potential, V
Ω	=	solid angle subtended by a disk, sr

Received 13 November 2001; revision received 8 May 2002; accepted for publication 15 May 2002.

*Senior Staff Scientist, Defense Technology Group, 9455 Towne Center Drive, Mail Stop W2076. Member AIAA.
†Division Manager, Defense Technology Group, 10260 Campus Point Drive, Mail Stop X1. Member AIAA.
‡Supervisor, Advanced Propulsion Technology Group, Thermal and Propulsion Engineering Section, 4800 Oak Grove Drive. Senior Member AIAA.
§Senior Research Associate, Department of Mechanical, Industrial, and Manufacturing Engineering. Member AIAA.

Introduction

SINCE its conception over three decades ago, the Hall thruster's[1] unique combination of high specific impulse and thrust-to-power ratio established it as a favored propulsion system for a variety of missions. In the former Soviet Union and, more recently, in Russia, over 70 stationary plasma thrusters have been employed on spacecraft since the early 1970s (Ref. 2). The October 1998 launch of the thruster with anode layer Russian Hall Electric Thruster Technology 1/Electric Propulsion Demonstration Module (RHETT1/EPDM) on the National Reconnaissance Organization Space Technology Experiment (NRO STEx) spacecraft also marked the first Western flight of a Hall-effect thruster (HET). Employment of this technology continues to be evaluated, worldwide, for orbit insertion to low Earth orbit,[3] geosynchronus Earth orbit,[4] and for more ambitious missions for the human exploration and development of space.[5]

A critical engineering issue in the employment of these devices is the potentially hazardous interaction of their exhausts with spacecraft systems. Such interactions have unfavorable consequences on mission lifetime and, in some cases, may jeopardize mission success. Quantitative evaluation of these effects is a complex task, with no comprehensive design tools or guidelines for the systems integrator in existence. The process of simulating a spacecraft's response during the operation of a Hall thruster usually begins with the generation of a plume map. Numerous two-dimensional computer models of HET plumes exist,[6–8] many of which have been compared to laboratory measurements. It is well known, however, that under laboratory conditions the exhaust from a HET may vary substantially from that in space due to the relatively high concentration of background neutrals in the vacuum chamber.[9] Consequently, accurate prediction of the plumes' interactions with a spacecraft in orbit relies heavily on scaling laws, which in turn depend on how well the conditions in space are known.

A two-dimensional simulation tool has been developed for the purpose of modeling electrostatic propulsion plumes and has been applied with great success to ion thrusters[10] and Hall thrusters[9] in the past. However, as in all other two-dimensional and three-dimensional plume codes in existence, results have never been compared to measurements obtained in space during the operation of a Hall thruster. This paper presents comparisons with the first data acquired during firings of eight stationary plasma thrusters (SPT100) on board the Express-A spacecraft. The two Russian communications satellites are currently in geosynchronous orbit. Ion-flux and induced torque measurements are compared with results from the two-dimensional plume code and the environment work bench (EWB), a three-dimensional spacecraft interactions simulation tool.

Two-Dimensional Plume Simulations

The plume map is generated using a two-dimensional, finite element (FE) code. The tool incorporates a revised selection of computer modules from the two-dimensional, electrostatic code Gilbert. The algorithms are part of a general production tool for plume mapping. The plume model consists of two main components: a Lagrangian algorithm for determining the expansion of the main beam and a particle-in-cell solver for computing the dynamics of the charge-exchange plasma.

Primary Ion Beam

The main beam exhausted from the thruster is assumed to be a collisionless, singly ionized, quasi-neutral plasma expanding under the influence of the (density-gradient) electric field. By comparison to heavy-particle motion, electrons reach dynamic equilibrium at much smaller characteristic times. The electron inertia term may, therefore, be neglected in the equation of motion. In the absence of electron–ion collisions and magnetic fields, conservation of momentum for the electrons is expressed by

$$m_e \frac{\mathrm{D}\boldsymbol{v}_e}{\mathrm{D}t} = e\nabla\phi - \frac{\nabla p}{n} = 0 \tag{1}$$

Under the assumption of ideal gas behavior and isothermal electrons, integration of Eq. (1) leads to the Boltzmann relation, which can be expressed in terms of the electric potential, as follows:

$$\phi(n, T_e) = T_e \ln(n/n_\infty) \tag{2}$$

Equation (2) is sometimes also known as the barometric potential law. With regard to the assumption of uniform electron temperature, measurements in the plume of various HETs reveal values that range between 6 and 11 eV in the near-field region (a few centimeters downstream of the exit), falling to less than 2–3 eV far from the thruster exit.[11–13] This variation in temperature suggests that a nonuniform temperature model that takes into account the effects of finite electron thermal conductivity would be more accurate. In light of the dominance of particle density gradients, however, an isothermal model is assumed, which is a better approximation under space conditions than in the laboratory where inelastic collisions with background neutrals will cool the electron. Unless otherwise stated, an effective temperature of 8 eV has been used in all HET plume simulations.

Ions are accelerated by the electric field, $\boldsymbol{E} = -\nabla\phi$, according to

$$m_i \frac{\mathrm{D}\boldsymbol{v}_i}{\mathrm{D}t} = -e\nabla\phi \tag{3}$$

Because the drift velocity of the ions $\boldsymbol{V}$ is much greater than their thermal velocity, the high-velocity ions are modeled as a fluid ($\boldsymbol{V} = \boldsymbol{v}_i$). The steady-state, conservation equations for mass and momentum are solved in two-dimensional (R–Z) geometry:

$$\nabla \cdot n\boldsymbol{V} = 0 \tag{4a}$$

$$m_i \boldsymbol{V} \cdot \nabla\boldsymbol{V} = -(\nabla p/n) \tag{4b}$$

The numerical algorithm for computing the expansion of the main ion beam is based on a Lagrangian approach. Discrete mass elements, otherwise known as "macroparticles" (not to be confused with the term associated with long polymer chains in ablation-fed pulsed plasma thrusters), are released from the thruster exit and tracked using fundamental trajectory kinematics. Under the assumption that variations in the electric field occur at a much larger timescale than ion transit times, the location of each macroparticle at time t is determined by

$$\boldsymbol{r} = \boldsymbol{r}_0 + \boldsymbol{V}(\boldsymbol{r}, t)t + \boldsymbol{a}(\boldsymbol{r}, t)t^2$$

$$\boldsymbol{V}(\boldsymbol{r}, t) = \boldsymbol{V}_0 + \boldsymbol{a}(\boldsymbol{r}, t)t, \qquad \boldsymbol{a}(\boldsymbol{r}, t) = [e\boldsymbol{E}(\boldsymbol{r}, t)/m_i] \tag{5}$$

At each successive time interval $t + \Delta t$ the density is updated using conservation of mass [Eq. (4a)]. With the updated density, the plasma potential [Eq. (2)] and electric field are recomputed for the next iteration. The iterative process uses a predictor–corrector method and ensues until ion trajectories are consistent with the local electric field. In steady state, the trajectories and particle locations at different times form a fictitious grid (Fig. 1). Particle density and velocity at each (fixed) Gilbert grid point is determined by linear interpolation using the values of the surrounding trajectory grid points.

The prediction of ion expansion from the Hall thruster requires knowledge of the conditions at the exit. In this effort, the boundary

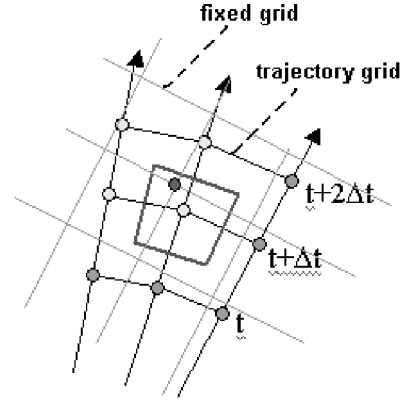

Fig. 1 Mesh arrangement formed by particle trajectories during the expansion of the main ion beam.

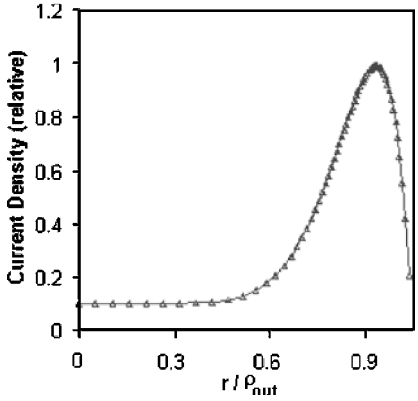

Fig. 2 Nondimensional current density profile specified at the thruster orifice.

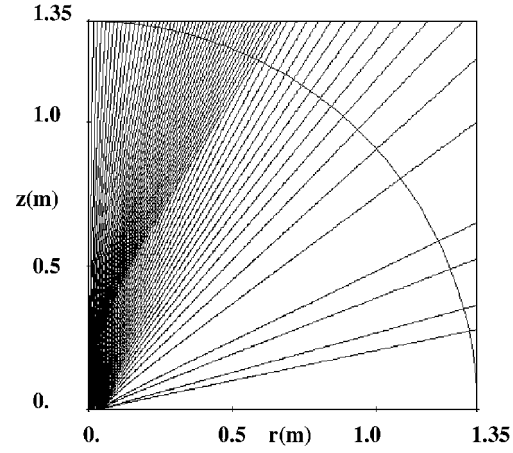

Fig. 3 Two-dimensional plume simulation of SPT100 showing ion trajectories.

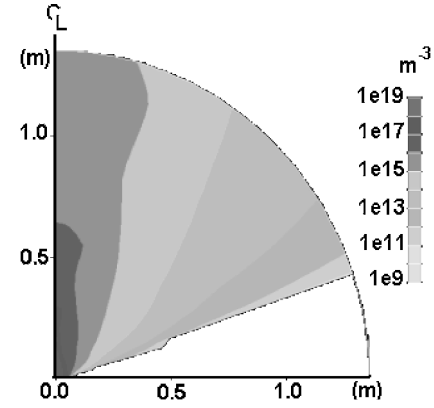

Fig. 4 Simulated SPT100 plume showing main beam ion particle density.

conditions have been estimated based on the performance of the SPT100 engine units measured as part of the Express-A acceptance test program. Specifically, the measurements on all four thruster units were obtained after 25-min operation at nominal parameters of 300 V (anode voltage) and 4.5 A (anode current) and produced thrust levels that varied between 86.6 and 80.2 mN. The total xenon mass flow rate through the thruster and cathode is not known, nor was the xenon mass flow rate from the acceptance tests provided. For other SPT100s, the total mass flow rate specification at 4.5 A of discharge current is 5.3 mg/s, although this may vary slightly from thruster to thruster. The cathode flow fraction is approximately 7%, and so the nominal anode flow rate is 4.9 mg/s (Ref. 14) (commonly applied to a variety of Hall thrusters). At the nominal value, and the average thrust value of 84 mN, the ion speed at the thruster exit is estimated as 19.06 km/s using

$$u_{i,\text{exit}} \approx f_T/\beta F_{A,\text{HET}} \tag{6}$$

The estimate also assumes that the propellant utilization β, the ratio of ion flow rate to anode flow rate, is 0.9. In a Hall thruster, both the current density and ion velocity vector vary along the exit. Figure 2 shows the (relative) radial profiles of ion flux implemented at the exit boundary. The profiles are based on previous measurements obtained during laboratory tests of a 4-kW Hall thruster.[9] The radial component of velocity was also varied based on evidence from tests of an SPT140 engine.[15] The implemented variation along the exit is linear with distance from the thruster centerline peaking to 8 km/s at the outer radius.

The Lagrangian modeling approach reduces the numerical noise[9] that is usually associated with particle-in-cell (PIC) algorithms, especially in cases where large changes in scale sizes are not adequately resolved, and when statistical particle fluctuations ("shot noise") overwhelm the physical forces. Moreover, without incredibly fine zoning and large numbers of particles, PIC is not accurate enough to prediction trajectories in problems with large-scale ratios, for example, fractions of a millimeter to several meters. However, unlike PIC, the fluid technique assumes a mono-energetic beam and may, therefore, lead to inaccuracies in the prediction of surface interactions such as sputtering by main-beam incident ions, that is, at plume angles less than 45–60 deg. A multi-energy beam could be simulated using a superposition of ion fluids, but was not performed in the present effort. Finally, PIC requires considerably longer computational times, for example, minutes of real time on an 800-MHz personal computer vs tens of hours of CPU time on parallel IBM SP/SP2 processors.[6] Figure 3 depicts computed ion trajectories for the SPT100, and Fig. 4 shows the computed ion density profile of the main beam. The thruster outer and inner radii are 5 and 3.5 cm from the origin, respectively.

Neutral Gas Density

The neutral gas density has two components in space: un-ionized (beam) particles from the thruster and un-ionized particles from the hollow cathode. The beam of neutrals from the thruster is computed using an annular anode gas flow model with isotropic emission from a ring. The profile of neutrals from the thruster is computed using two disk emissions defined by the solid angles $\Omega(\bar{r},\bar{z})|_\rho$ subtended by each disk and subtracting the smaller from the larger:

$$n_{0,\text{HET}}(\bar{r},\bar{z}) = \frac{2F_{0,\text{HET}}}{m_i u_{0,\text{HET}} \pi\left(\rho_{\text{out}}^2 - \rho_{\text{in}}^2\right)}\left[\Omega(\bar{r},\bar{z})|_{\rho_{\text{out}}} - \Omega(\bar{r},\bar{z})|_{\rho_{\text{in}}}\right] \tag{7}$$

Further elaboration on Eq. (7) is provided in the Appendix. The effective mean speed of the neutrals at the thruster exit is assumed to be the average component of velocity in the axial direction for a one-sided Maxwellian distribution function. The thruster neutrals are assumed to be at wall temperatures (~700 K), yielding a value of 168 m/s. The flow rate of neutrals from the thruster exit is estimated using the anode flow rate and propellant utilization:

$$F_{0,\text{HET}} = F_{i,\text{HET}}(1-\beta) \tag{8}$$

The density of neutrals at the thruster exit is then found to be $3.3e18\ \text{m}^{-3}$.

The hollow cathode is offset by a distance r_{HC} from the thruster. Its axial location is assumed to be at $z = 0$. The isothermal neutrals are emitted isotropically from the neutralizer. Their speed is estimated based on the same assumptions used for the thruster neutrals with a slightly higher wall temperature (~810 K), yielding a corresponding speed of 180 m/s. Their distribution is estimated based on

$$n_{0,\text{HC}}(r,z) = \frac{F_{0,\text{HC}}}{\pi r_{\text{HC}}^2 m_i u_{0,\text{HC}}} \begin{cases} \dfrac{z/r_{\text{HC}}}{[1+(z/r_{\text{HC}})^2]^{\frac{3}{2}}}, & r/r_{\text{HC}} \le 1 \\ \dfrac{z/r_{\text{HC}}}{[(r/r_{\text{HC}})^2+(z/r_{\text{HC}})^2]^{\frac{3}{2}}}, & r/r_{\text{HC}} > 1 \end{cases} \tag{9}$$

Based on SPT100 drawings in the Russian reports,[16,17] the distance of the cathode from the centerline is 14.5 cm. To simulate

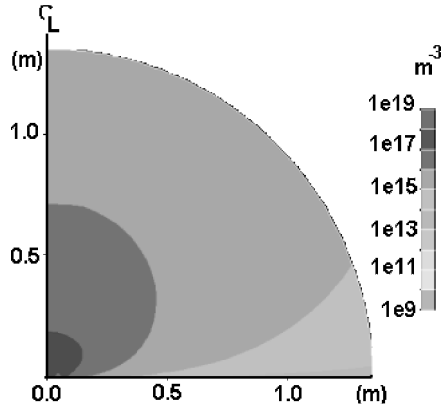

Fig. 5 Neutral particle density profile used in the SPT100 plume simulations.

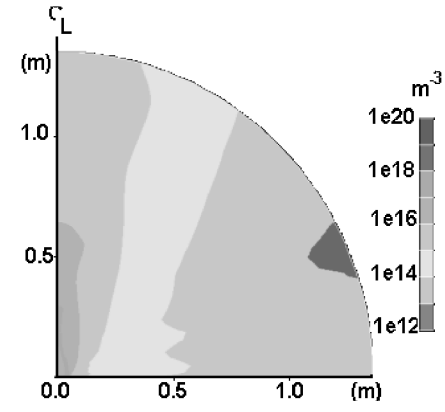

Fig. 6 Simulated SPT100 plume showing total ion particle density.

space conditions, no contribution from background neutrals was added. A two-dimensional map of the total neutral particle density used in the SPT100 simulations is shown in Fig. 5.

Neutral–Ion Interactions

Fast ions from the main beam undergo charge-exchange (CEX) with neutral particles, resulting in slow-moving ions and fast-moving neutrals,

$$_{\text{fast}}\text{Xe}^{+} + {}_{\text{slow}}\text{Xe} \rightarrow {}_{\text{slow}}\text{Xe}^{+} + {}_{\text{fast}}\text{Xe} \tag{10}$$

CEX is computed using a two-dimensional PIC code. The rate of CEX-ion production is determined by

$$\dot{n}_{\text{CEX}} = nV\sigma_{\text{CEX}}n_0 \tag{11}$$

In contrast to the approach for the calculation of the main beam ions, where direct use of Eq. (2) provides the potential, the PIC algorithm solves the two-dimensional Poisson's equation on an FE grid and iterates until steady-state CEX densities and potentials are self-consistent. The plasma density in Poisson's equation is the sum of the main beam and CEX densities. The first (computed by the Lagrangian method) and the preceding prescribed neutral gas profile are used as input for the calculation. Based on the fact that the density of CEX ions is more than two orders of magnitude less than of the main-beam ions, no correction is made to the latter as a result of the first. The simulated SPT100 plume showing total ion particle density appears in Fig. 6. In all ensuing comparisons with computed values (using xenon) a constant value of $5.5e{-}19$ m^2 has been assumed for the CEX collision cross section. The value is based on measurements taken by Pullins et al.[18] for 0–500-V ions.

Plume Modeling and Comparisons

In the past few years, the two-dimensional plume code has been applied successfully in a variety of electrostatic propulsion plume simulations. Modeling of the Deep Space 1 ion thruster plume showed reduced CEX ion concentrations in space compared to the laboratory, confirming the enhancing effect of vacuum chamber neutrals on CEX ion production.[10] Simulations of 4-kW Hall thruster plumes also provided critical insight into ion-neutral collision processes that occur in the laboratory. Guided by empirical observations, these calculations exposed neutral-ion processes, not previously modeled, that produce highly energetic ions (>100 V) at large angles (in addition to the low-energy CEX ions expected to be present there).[9] In certain cases, these ions can be the dominant high-energy particles at large angles relative to the thrust direction and may, therefore, contribute substantially to the sputtering of spacecraft surfaces.

More recently, measurements have been received from two Russian geosynchronus communication satellites, Express-A 2 and A 3 (Refs. 16 and 17). Both spacecraft were launched aboard Proton launch vehicles from the Baikonur Cosmodrome in Kazakhstan. Express-A 2 was launched on 12 March 2000 and is currently

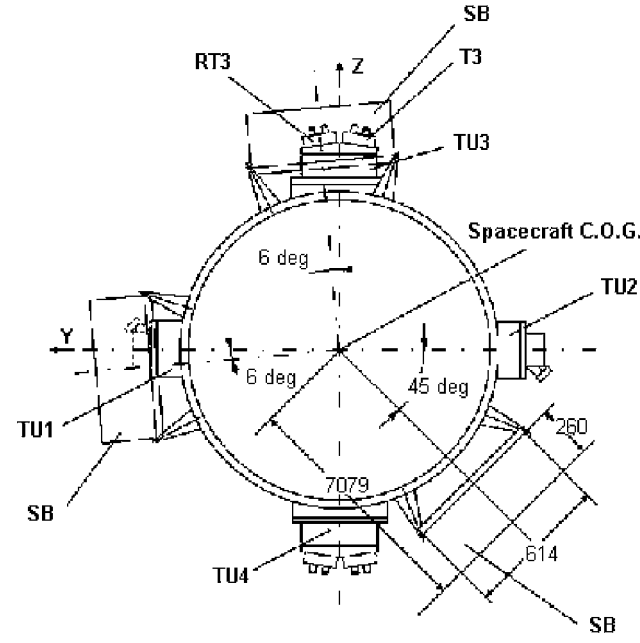

Fig. 7 Orbital control thruster units on board the Express-A spacecraft (top view).

on-orbit, providing telecommunication services for Russian television and network operations. Express-A 3 was launched on 24 June 2000 to provide high-speed Internet access to the Middle East and Africa from Europe. Both satellites employ eight SPT100 engines for station keeping. More specifically, the propulsion system for each spacecraft consists of four orbital control thruster units, the xenon feed unit, three xenon storage units, and the power-processing unit. Each thruster control unit was provided by Fakel Enterprises of Kaliningrad, Russia, and contains two redundant SPT100 Hall thrusters. Each thruster has two redundant cathodes, necessary propellant valves, flow restrictors, and thermo-throttles. Each thruster control unit is designated as TU1, TU2, TU3, or TU4, and they are arranged according to Fig. 7 (bottom). The two thrusters on each unit are designated based on whether each is the primary or redundant thruster (T or RT). For example, the primary thruster of TU4 is designated T4 and the redundant thruster is RT4. TU1 and TU2 are used for east–west station keeping and TU3 and TU4 are used for north–south station keeping. Each thruster within the thruster control unit is positioned with a ~6-deg angle with respect to ideal north–south or east–west direction passing through the spacecraft center of gravity.

Comparisons with Data from Express-A 2

Measurements from two ion-flux sensors and three electric field sensors (designated as DRT and DEP, respectively) on board the Russian Express-A 2 spacecraft were provided. Values from one ion-flux sensor were used, those of the DRT1. The second sensor

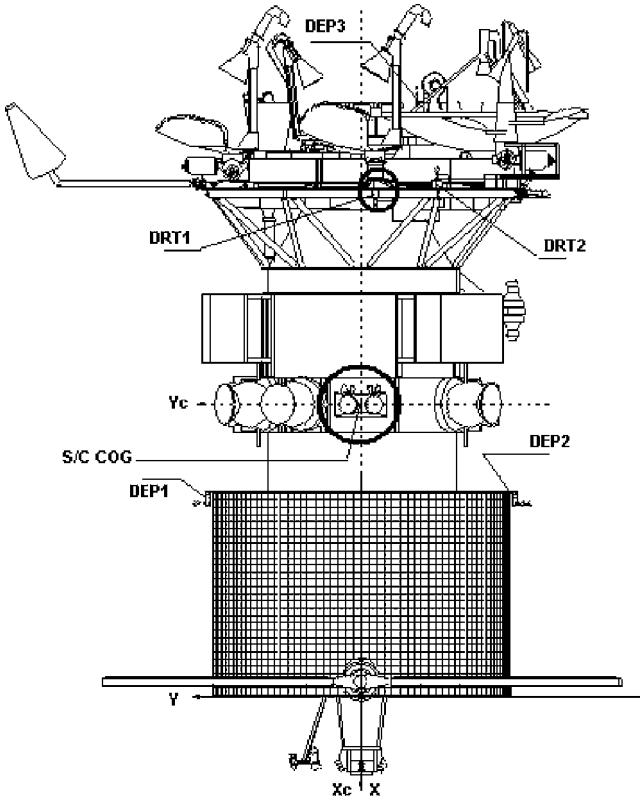

Fig. 8 Side view of the Express-A 2 spacecraft; circled are the ion flux sensor (small circle) and TU4 SPT100 unit (large circle).

(DRT2) is positioned under a multilayer insulation (MLI) blanket and did not provide useful information. The positions of DRT1 and TU4 on the Express-A 2 spacecraft are shown in Fig. 8. The DRT1 sensor is at a distance of 1.352 m from RT4 (right thruster), at an angle of approximately 80 deg relative to the *Xc* axis. Signals during this thruster's operation have been used for comparisons.

The precise value of the mass flow rate during thruster operation was not known. Two different simulation cases of plume maps were initially performed, distinguished by two mass flow rate values: 4.9 and 5.3 mg/s for the thruster and 0.49 and 0.371 mg/s, respectively, for the cathode neutralizer. The plume model computes the ion current density at the position of the DRT1 detector to be 19.9 mA/m^2 for the low flow rate case (4.9 mg/s), and 26.9 mA/m^2 for the higher flow rate (5.3 mg/s). The DRT1 signals indicated significant fluctuations, 16–41 mA/m^2, during a 2-h operation of RT4 on 13 April 2000 (Fig. 9a). Data from momentary firings of the same thruster on different dates also show noticeable variations. The sensors registered values that ranged between 13–25 mA/m^2 (Fig. 9b) on 16 March 2000 and 18–52 mA/m^2 on 5 May 2000 (Fig. 9c). Signals from the T4 thruster during continuous operation on 12 April 2000 were characterized by reduced fluctuations with an average value of about 13 mA/m^2. According to Russian engineers, the large ion-flux variation during the operation of RT4 may be due to initial outgassing of the chamber walls commonly taking place during the first firings of these thrusters. This additional mass from the chamber walls would indeed alter the effective mass flow rate during operation and, therefore, the observed ion flux.

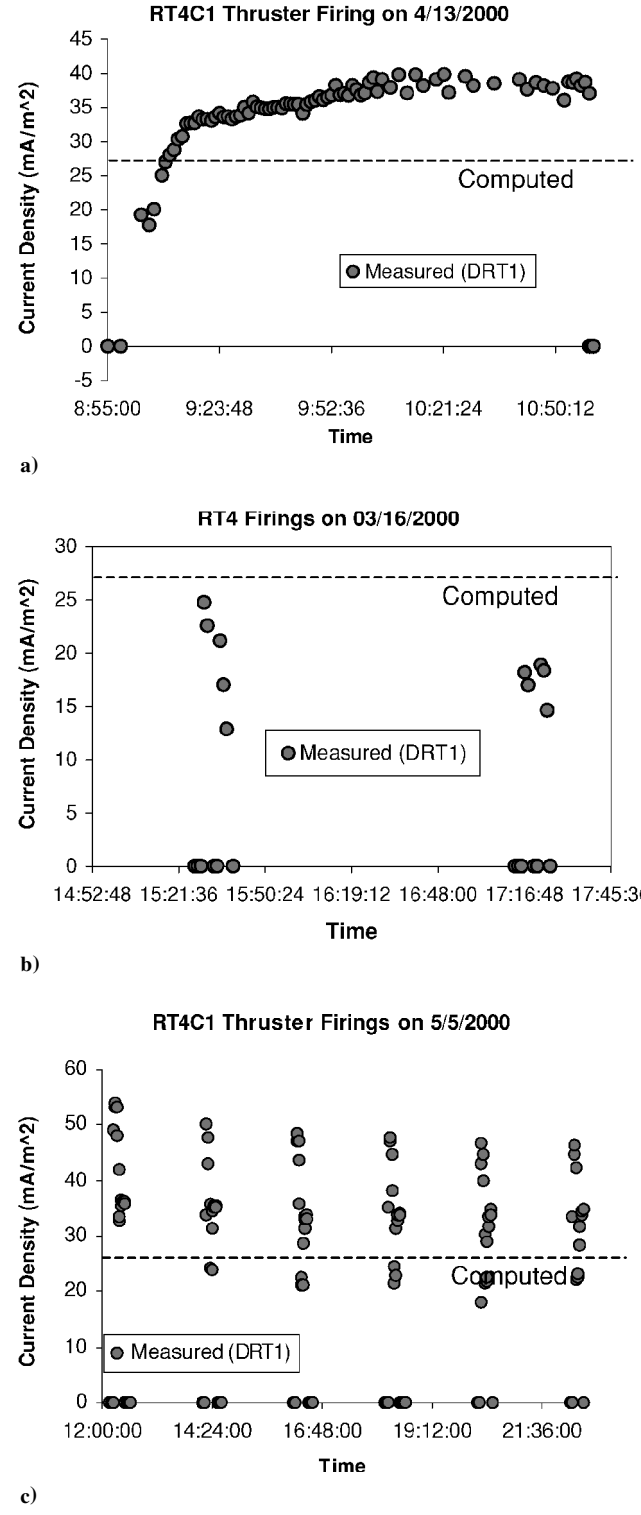

Fig. 9 Comparison between computed and measured currents.

Comparisons with Data from Express-A 3

Measurements from the Express-A 3 spacecraft were also provided. The values were registered by two ion-flux sensors (DRT1 and DRT2) located at the sides of the (rotating) solar arrays (Fig. 10). These instruments consist of two three-grid retarding potential analyzers (RPA) used to measure ion current density and energy. DRT3-1, the sensor located at the same position as the DRT1 on the Express-A 2 satellite, is a four-grid RPA and registered zero values. Contrary to the Express-A 2 satellite, the second sensor, DRT3-2, (positioned under the MLI) provided nonzero readings that could not be compared to computed values due to the orientation of the sensor relative to the thruster (upward), as well as possible interference by other spacecraft structures.

Results from the Express-A 3 simulations and comparisons with measurements are presented in Figs. 11–14. A mass flow rate of 5.3 mg/s for the thruster and 0.371 mg/s for the cathode neutralizer were used as input values to the model. The plume model computes an ion current density at the position of the DRT1 detector (3.542 m away) of 41.6 μA/cm^2 at 0 deg (with respect to the axis of symmetry) and 35 μA/cm^2 at 10 deg (Fig. 11). Note that when the solar array angle is 0 deg (see Fig. 10) the DRT1 sensor is approximately 3.8 m away from the SPT exit and 7 deg left and 3 deg down from the thruster axis. The values in Fig. 11 were obtained during firings of the T4 SPT100 on 7 June 2000. During three different RT4 firings,

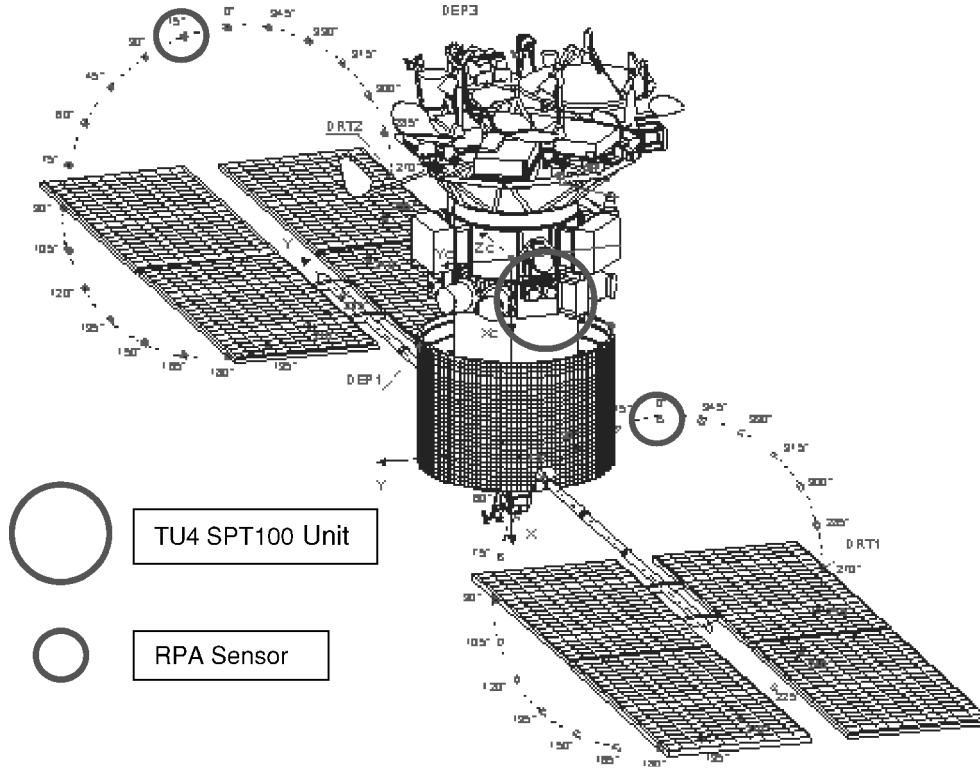

Fig. 10 Express-A 3 spacecraft showing thruster and RPA locations.

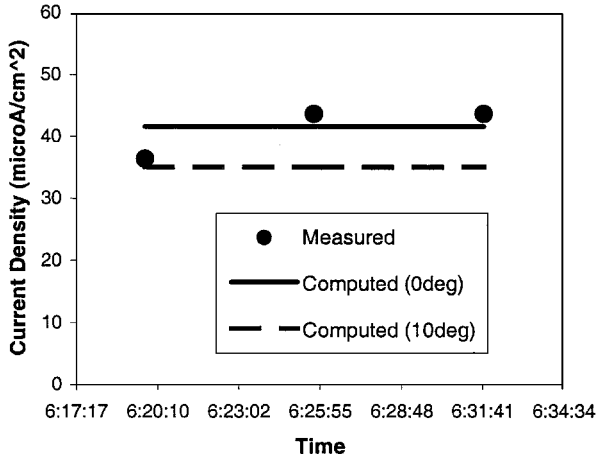

Fig. 11 Comparison between computed (at 0- and 10-deg plume angles) and DRT1 measurements of current density.

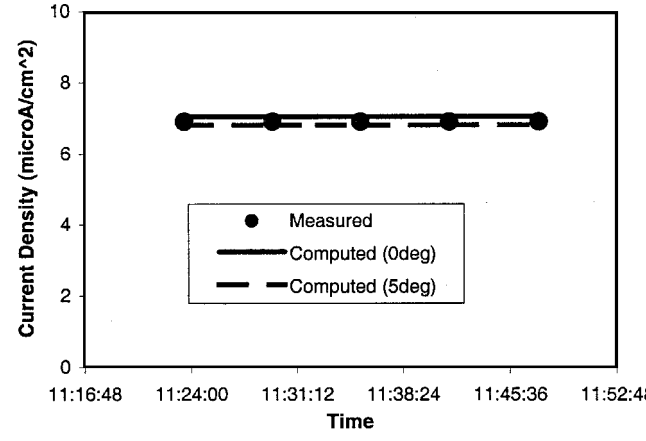

Fig. 12 Comparison between computed (at 0- and 5-deg plume angles) and DRT2 measurements of current density.

the values measured by the sensor, when the solar array angle was at 0 deg with respect to the *Xc* axis, varied from 36 to 54 μA/cm^2. Additional comparisons with values registered by the DRT2 sensor are presented in Fig. 12 during operation of the RT3 SPT100. When the solar array angle is 15 deg (Fig. 10), the DRT2 sensor is approximately 8.8 m away from the RT3 exit, 3 deg right and 1.5 deg down from the thruster axis. The measurements in Fig. 12 were acquired during firings of the RT3 SPT100 on 9 July 2000. The energy spectra in Fig. 13 suggest a high-energy peak of between $E/q = 233.3$ and 247.1 V at this location. The computed value is $E/q = 229$ and 234 V for plume angles of 0 and 10 deg, respectively. The RPA values shown in Fig. 13 were obtained during firings of the T4 SPT100 on 7 June 2000, when the solar array angle was 0 deg (see Fig. 10).

All (useful) ion-flux measurements from both spacecraft, taken at various times during the acquisition period, and at different locations with respect to the center of gravity, were compiled and scaled ($\sim 1/r^2$) down to a 1-m radius. Although the accuracy of the scaling with the inverse of the distance squared may not be confirmed in space, it is assumed that no other unknown physical mechanisms existed during the firings that may have perturbed the

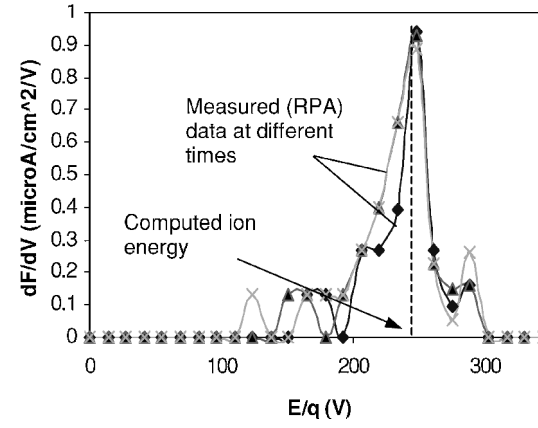

Fig. 13 Computed value of the main beam ion energy and measured energy spectra onboard the Express-A 3 spacecraft from the DRT1 sensor.

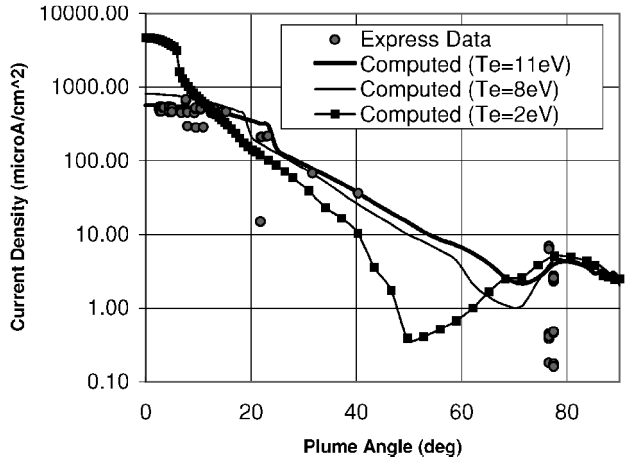

Fig. 14 Comparison between current density measurements onboard the Express-A spacecraft and computed values using the two-dimensional plume code at a radius of 1 m.

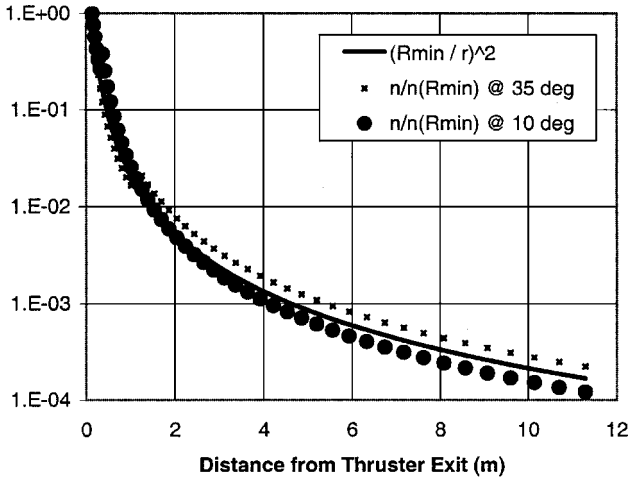

Fig. 15 Main beam plasma density computed as a function of distance (starting from a location close to the thruster exit, R_{min} = 15 cm); shown are computed values for two plume angles.

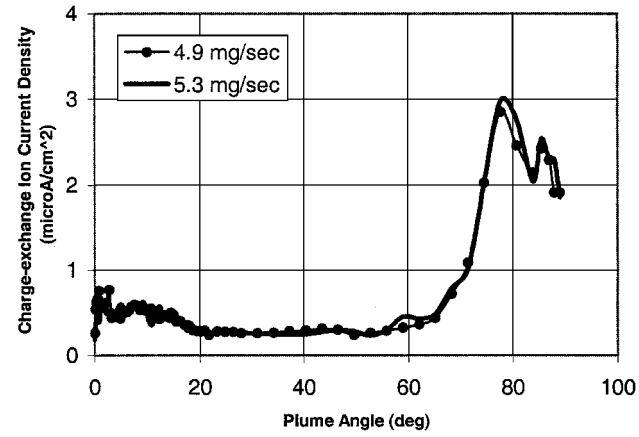

Fig. 16 Computed CEX ion current density as a function of plume angle, 1 m downstream of the thruster exit; profiles for two thruster mass flow rates are shown.

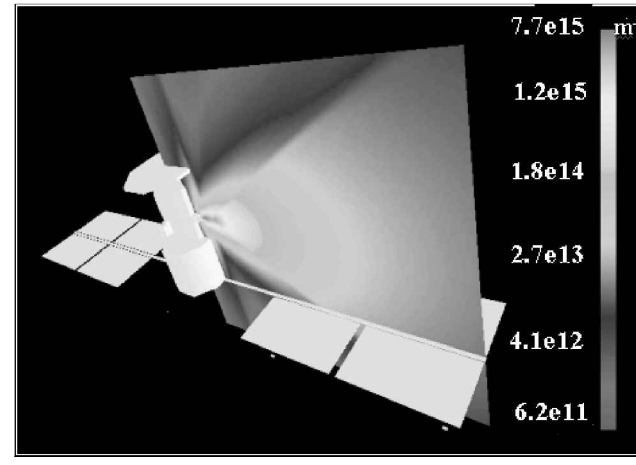

Fig. 17 EWB-generated model of the Express-A spacecraft showing plume ion density profile during operation of RT4 SPT-100 thruster.

expected variation with distance. With regard to the model, Fig. 15 confirms the dependence of density on $\sim 1/r^2$. Figure 14 shows a comparison between these measurements and computed values as a function of plume angle. As alluded to earlier, although the precise nominal mass flow rate during operation of the thrusters is not known, computed values were produced using 5.3 mg/s of anode flow rate. The comparison suggests that the model overpredicts the mean measured value by approximately 20% for angles less than 20 deg. The effective electron temperature during operation, however, is also unclear. The value of 8 eV used here may have been higher, as was also shown by laboratory measurements.[13] The choice of such a high electron temperature for the plume model requires further justification. Equation (2) suggests that the ratio of plasma potential to electron temperature goes to zero far away from the exit, as the plasma density approaches n_∞. Both the simulations and the simple scaling suggest that the plasma density drops by more than two orders of magnitude within a few tens of centimeters away from the thruster exit. Therefore, in view of both the magnitude and (more important) the gradients of the plasma potential at distances greater than 20–50 cm, the high-temperature choice introduces a relatively small error on the ion trajectories. In contrast, close to the exit where the electron temperature is indeed high, as confirmed by numerous measurements,[12,13] a low-value choice ($\sim$2 eV) would have a more erroneous effect on the expanding plasma because the largest electric forces are concentrated close to the thruster exit. Consequently, in view of the dominant role that the near-field forces have on the evolution of the plume, the high-temperature choice appears more reasonable. As alluded to earlier, a more accurate calculation would incorporate the effects of nonuniform temperature using energy conservation considerations with a proper model of thermal conductivity for the electrons. For comparison purposes, Fig. 14 also depicts computed values for an electron temperature of 11 and 2 eV. With regard to the values at the larger angles, the comparison is inconclusive due to the large spread in the data. As expected under space conditions, the contribution of CEX ions is minimal for angles less than $\sim$60 deg (Fig. 16).

Spacecraft Interactions with the SPT100 Plume

Plume interactions with spacecraft subsystems, in three dimensions, are assessed using the EWB. The three-dimensional spacecraft interactions computer tool has a variety of modeling capabilities, including surface erosion and redeposition, heating, and optical emissions.[19,20] For Hall (and ion) thrusters, the maps produced with the two-dimensional plume tool are incorporated into EWB, which, in turn, interpolates it symmetrically in the three-dimensional space. Figures 17 and 18 show the model spacecraft, ion density distribution in an x–z plane, and computed erosion of the solar array panels during firing of the T4 thruster. For comparison purposes, a model to determine the induced torques on the spacecraft during thruster operation was implemented. The model accounts for contributions from the thrust and from the impingement of the exhaust on surfaces:

$$\boldsymbol{\Gamma} = \sum_T \Delta \boldsymbol{R}_T \times (-\boldsymbol{f}_T) + \sum_j \Delta \boldsymbol{R}_j \times \boldsymbol{f}_j \qquad (12)$$

Measurements for both the T4 and RT4 thrusters are shown in Fig. 19. The oscillation asymmetry induced by the high torque values at 240-deg solar array (SA) angle suggests that the back and front

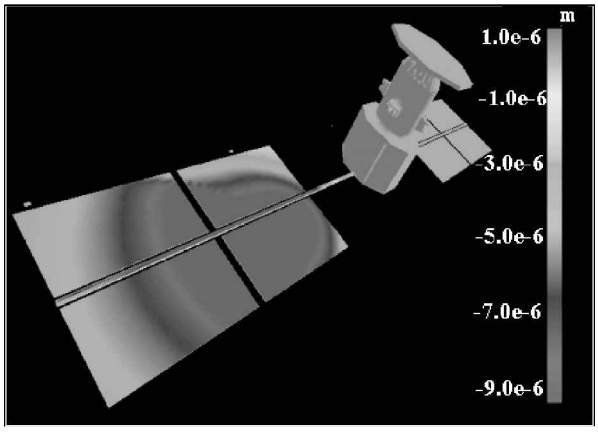

Fig. 18 Surface erosion (negative numbers) and deposition depths (positive numbers) due to sputtering as calculated by EWB during operation of the T4 SPT100.

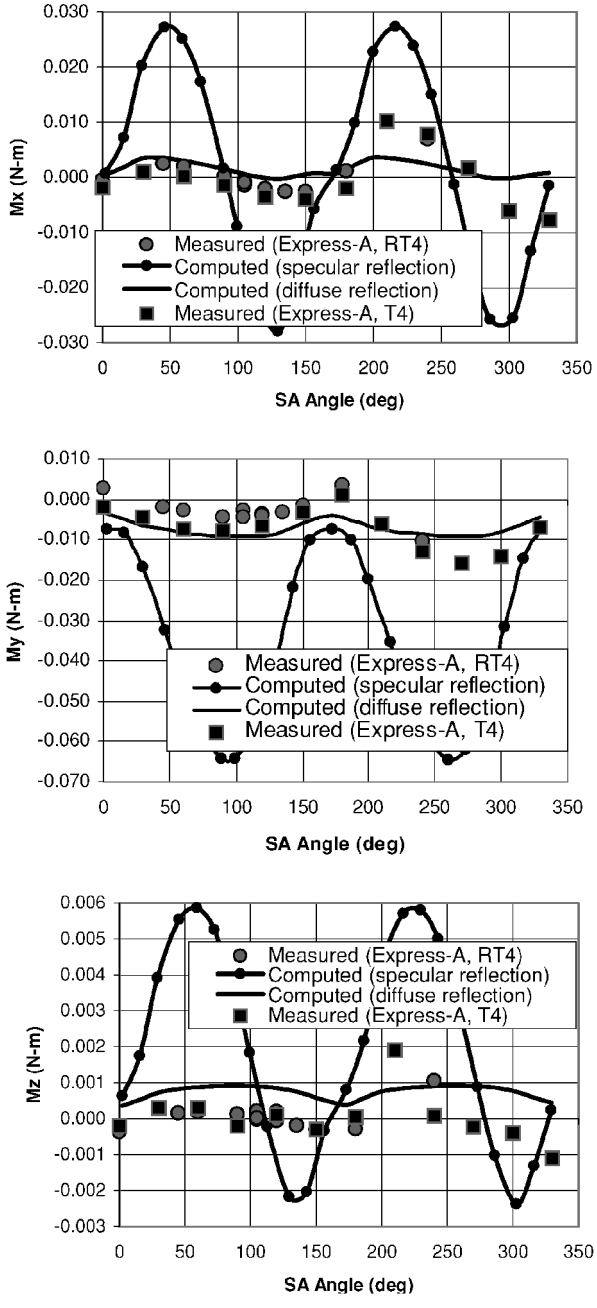

Fig. 19 Comparison between computed and measured torques induced by firings of the RT4 SPT100; measurements were taken during a rotation of the SA.

surfaces of the array may have distinct reflective properties. This has not yet been confirmed for the Express-A spacecraft. Reports on the previous spacecraft series Express indicated that, indeed, the back and front surfaces of that spacecraft had different properties. In the model, the contribution from plume impact is computed using two limiting cases: specular (elastic) reflection from the surface (colliding particle is reflected with the same speed and incidence angle equals the reflection angle) and fully diffused reflection (also known as complete accommodation). The incremental force imparted on an elemental surface dA by incident particles is equal to the momentum flux on that surface:

$$\mathrm{d}\boldsymbol{f} = nm_i(\boldsymbol{u}\cdot\mathrm{d}\boldsymbol{A})\boldsymbol{u} \tag{13}$$

In the case of specular reflection, the total force is normal to that surface with $-\boldsymbol{u}_{\text{inc}}\cdot\boldsymbol{n} = \boldsymbol{u}_{\text{ref}}\cdot\boldsymbol{n}$,

$$\begin{aligned}\boldsymbol{f}_s &= nm_i\lfloor(\boldsymbol{u}_{\text{out}}\cdot\boldsymbol{n})\boldsymbol{u}_{\text{ref}} + (\boldsymbol{u}_{\text{inc}}\cdot\boldsymbol{n})\boldsymbol{u}_{\text{inc}}\rfloor A \\ &= -2nm_i A(\boldsymbol{u}_{\text{inc}}\cdot\boldsymbol{n})^2\boldsymbol{n}\end{aligned} \tag{14}$$

For fully diffused reflection, the force is in the direction of the velocity of the incoming particles with the reflected particles assumed to have negligible velocity. Then, the force on the impacted surface is given by

$$\boldsymbol{f}_d = nm_i A(\boldsymbol{u}_{\text{inc}}\cdot\boldsymbol{n})\boldsymbol{u}_{\text{inc}} \tag{15}$$

Figure 18 illustrates the computed (limiting) torques, induced by the T4 SPT100, as a function of SA angle (see Fig. 10 for SA angle definition). The comparison suggests good overall qualitative agreement. Quantitatively, comparison with the model for the x and y moments at angles less than ~180 deg suggest that the SA surface exposed to the plume within these angles is closer to diffusive than specular. Conversely, the behavior of the data at SA values greater than ~180 deg indicates that the opposite surface has reflective properties that lie between the two limits, and, therefore, appropriate accommodation coefficients would have to be implemented in the model before direct comparisons can be performed. That the diffusive model overestimates the data for the x and z moments, and underestimates the values for the y moment, is questionable. The uncertainties involved with acquisition of these measurements remain unknown, as do the exact details of the onboard attitude control system (ACS) instrumentation.

Conclusions

The first flight measurements on SPT have been obtained from the Russian Express-A satellite and have been compared with results produced by two-dimensional plume and three-dimensional spacecraft interactions codes. The plume comparisons yielded good quantitative agreement with ion-flux measurements for the main ion beam, at various locations from the thruster, assuming a constant electron temperature of 8 eV. Comparison with a larger portion of the ion-flux data during rotation of the solar arrays, scaled down to 1 m from the thruster, suggest better agreement for electron temperature of 11 eV. Electron temperatures in the range of 8–11 eV have been measured in the past, in the near-field region, during ground tests of SPT-like engines. Computed values also lie within the large spread observed onboard Express-A 2 at the larger angles, where most of the CEX ions are concentrated. The spread in the data suggests that the effective mass flow rate may have varied during thruster operation. Telemetry data, however, did not provide any pertinent information on the mass flow rate during firings. After incorporating the two-dimensional plume map into the three-dimensional spacecraft interactions tool EWB, induced torque calculations during rotation of the solar arrays also produced good qualitative agreement with ACS measurements. The calculations assumed two limiting cases, specular and fully diffused reflection of ions from surfaces. The data lie between the two computed cases for SA angles greater than ~180 deg, with closer agreement of the measurements with computed values based on the fully diffused model. Both observations suggest that the back and front surfaces of the arrays have different reflective properties with one closer to a rougher surface than the other. This was indeed the case in a previous Russian spacecraft series Express.

Appendix: Neutral Particle Density Distribution in the Plume

The profile of neutrals from the HET is computed using two disk emissions and subtracting the smaller from the larger. By the use of the nondimensional coordinates,

$$\bar{r} \equiv r/\rho, \qquad \bar{z} \equiv z/\rho \tag{A1}$$

the density profile for a cylindrical channel radius ρ is calculated by the geometrical relations,

$$\theta_1(\bar{r},\bar{z}) = a\tan\left(\frac{\bar{r}+1}{\bar{z}}\right) - a\tan\left(\frac{\bar{r}}{\bar{z}}\right)$$

$$\theta_2(\bar{r},\bar{z}) = -a\tan\left(\frac{\bar{r}-1}{\bar{z}}\right) + a\tan\left(\frac{\bar{r}}{\bar{z}}\right)$$

$$\theta_3(\bar{r},\bar{z}) = a\sin\left(\sqrt{\frac{1-\bar{x}^2}{1+\bar{r}^2-2\bar{r}\bar{x}+\bar{z}^2}}\right) \tag{A2}$$

where

$$\bar{x}(\bar{r},\bar{z}) \equiv x(\rho,r,z)/\rho$$

$$= (1/2\bar{r})\left[1+\bar{r}^2+\bar{z}^2-\sqrt{1+(\bar{r}^2+\bar{z}^2)^2+2(\bar{z}^2-\bar{r}^2)}\right]$$

$$\bar{r} > 0 \tag{A3}$$

Equations (15–A2) allow for the determination of the solid angle $\Omega(\bar{r},\bar{z})$ subtended by the disk at the end of the channel. The particle density is then calculated using the neutral flow rate, the neutral speed at the thruster exit, the particle mass, and the solid angle, as follows:

$$\Omega(\bar{r},\bar{z}) = \frac{1}{2}\sqrt{\left[1-\frac{\cos(\theta_1)+\cos(\theta_2)}{2}\right][1-\cos(\theta_3)]} \tag{A4}$$

$$n_{0,\mathrm{cyl}}(\bar{r},\bar{z}) = \frac{2F_0}{m_i u_0 \pi \rho^2}\Omega(\bar{r},\bar{z}) \tag{A5}$$

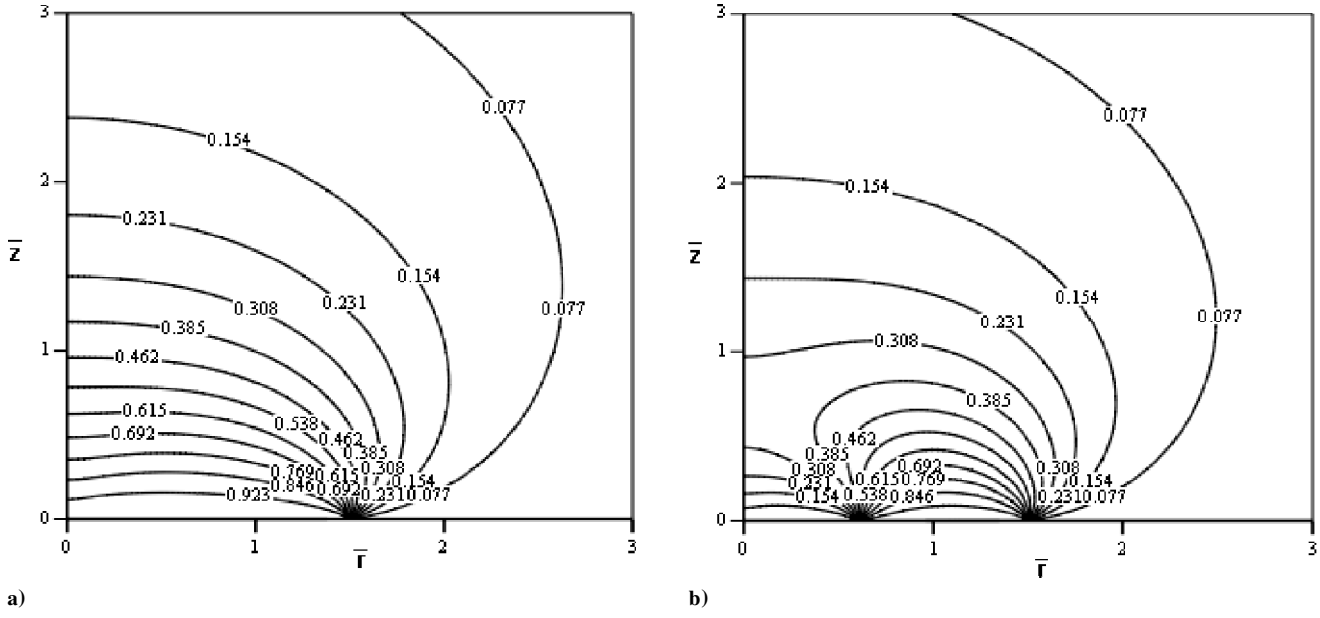

a) b)

Fig. A1 Ratio of neutral particle density in plume over value at the exit for a) disk and b) ring.

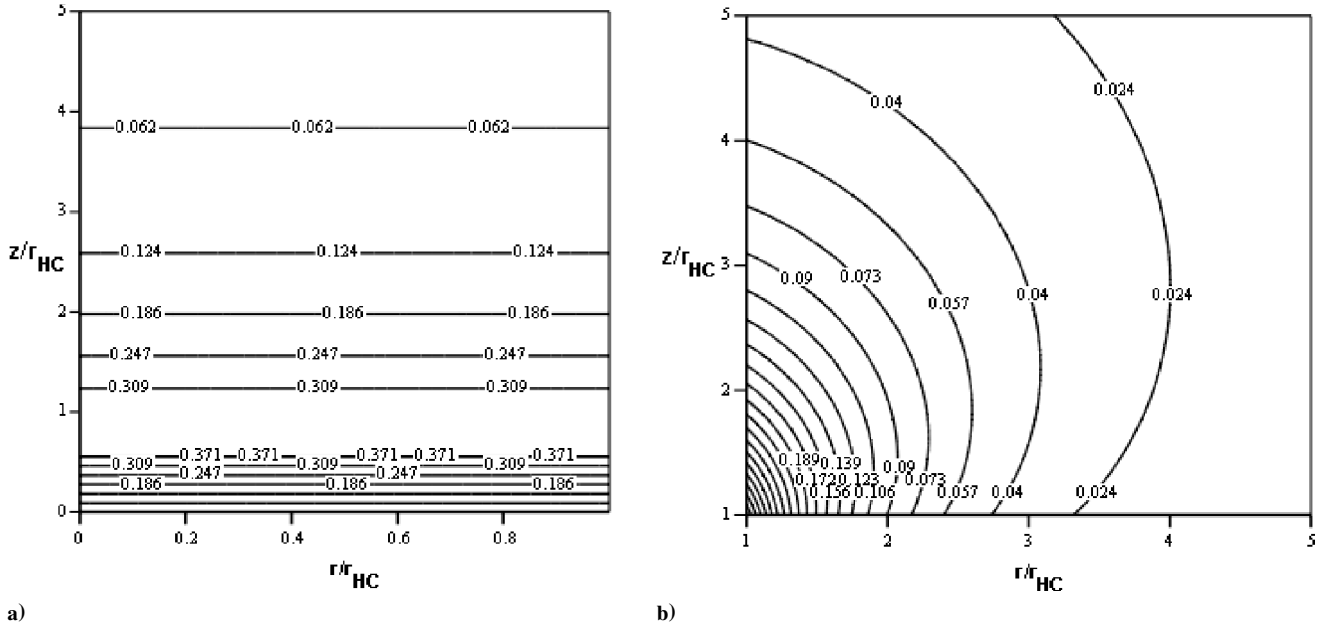

a) b)

Fig. A2 Nondimensional neutral particle density profile in the plume due to emission from the hollow cathode.

To account for the ring emission of neutrals from the HET, Eq. (A4) takes the form

$$n_{0,\mathrm{HET}}(\bar{r},\bar{z}) = \frac{2F_{0,\mathrm{HET}}}{m_i u_{0,\mathrm{HET}} \pi \left(\rho_{\mathrm{out}}^2 - \rho_{\mathrm{in}}^2\right)} [\Omega(\bar{r},\bar{z})|_{\rho_{\mathrm{out}}} - \Omega(\bar{r},\bar{z})|_{\rho_{\mathrm{in}}}] \tag{A6}$$

The (nondimensional)neutral density profile for a disk ($\rho = 1.5$ cm) is shown in Fig. A1a. The profile is appropriate for ion thruster simulations. For a Hall thruster (with $\rho_{\mathrm{in}} = 0.6$ cm and $\rho_{\mathrm{out}} = 1.5$ cm), the profile is illustrated in Fig. A1b.

Figure A2 illustrates the density profile assumed for the neutral particles exhausted from the hollow cathode. The emission assumes that the distribution is radially uniform for $r/r_{\mathrm{HC}} \leq 1$ with $1/z^2$ variation in the axial direction as shown in Fig. A2a. For $r/r_{\mathrm{HC}} > 1$, the inverse-squared variation is retained in both directions (Fig. A2b).

Acknowledgments

The authors wish to acknowledge Todd Peterson and Robert Jankovsky of the NASA Glenn Research Center for making the Express/SPT100 reports and data available.

References

[1]Morozov, A. I., Esipchuk, Yu. V., Tilinin, G. N., Trofimov, A. V., Sharov, Yu. A., and Shchepkin, G. Ya., "Plasma Acceleration with Closed Electron Drift and Extended Acceleration Zone," *Soviet Physics—Technical Physics*, Vol. 17, No. 1, 1972, pp. 32–37.

[2]Bober, A. S., and Maslennikov, N. A., "SPT in Russia—New Achievements," International Electric Propulsion Conf., IEPC Paper 1995-06, Sept. 1995.

[3]Oleson, S. R., "Electric Propulsion for Low Earth Orbit Communications Satellites," International Electric Propulsion Conf., IEPC Paper 97-102, Aug. 1997.

[4]Oleson, S. R., and Myers, R. M., "Advanced Propulsion for Geostationary Orbit Insertion and North–South Station Keeping," *Journal of Spacecraft and Rockets*, Vol. 34, No. 1, 1997, pp. 22–28.

[5]Oleson, S. R., and Sankovic, J. M., "Advanced Hall Electric Propulsion for Future In-Space Transportation," NASA TM-2001-210676, 2001.

[6]VanGilder, D. B., Boyd, I. D., and Keidar, M., "Particle Simulations of a Hall Thruster Plume," *Journal of Spacecraft and Rockets*, Vol. 37, No. 1, 2000, pp. 129–136.

[7]Oh, D., and Hastings, D., "Experimental Verification of a Particle-in-Cell–Discrete Simulation Monte Carlo Model for Hall Thruster Plumes," AIAA Paper 96-3196, July 1996.

[8]Samanta Roy, R. I., Hastings, D. E., and Gatsonis, N. A., "Numerical Study of Spacecraft Contamination and Interactions by Ion-Thruster Effluents," *Journal of Spacecraft and Rockets*, Vol. 33, No. 4, 1996, pp. 535–542.

[9]Katz, I., Jongeward, G. A., Davis, V. A., Mandell, M. J., and Mikellides, I. G., "Hall Effect Thruster Plume Model Including Large-Angle Elastic Scattering," AIAA Paper 2001-3355, July 2001.

[10]Davis, V. A., Katz, I., Mandell, M. J., Brinza, D. E., Henry, M. D., Wang, J. J., and Young, D. T., "Ion Engine Generated Charge Exchange Environment: Comparison Between NSTAR Flight Data and Numerical Simulations," Paper AIAA 2000-3529, July 2000.

[11]Kim, S. W., Foster, J. E., and Gallimore, A. D., "Very-Near-Field Plume Study of a 1.35-kW SPT-100," AIAA Paper 96-2972, July 1996.

[12]Fife, J. M., "Hybrid PIC-Modeling and Electrostatic Probe Survey of Hall Thrusters," Ph.D. Dissertation, Dept. of Aeronautics and Astronautics, Massachusetts Inst. of Technology, Cambridge, MA, Sept. 1998.

[13]Haas, J. M., and Gallimore, A. D., "Investigation of Internal Ion Number Density and Electron Temperature Profiles in a Laboratory-Model Hall Thruster," AIAA Paper 2000-3422, July 2000.

[14]Manzella, D., Jankovsky, R., Elliott, F., Mikellides, I. G., Jongeward, G. A., and Allen, D. "Hall Thruster Plume Measurements On-Board the Russian Express Satellites," International Electric Propulsion Conf., IEPC Paper 2001-327, Oct. 2001.

[15]Pollard, J. E., and Beiting, E. J., "Ion Energy, Ion Velocity, and Thrust Vector Measurements with the SPT-140 Hall Thruster," 3rd International Conf. on Spacecraft Propulsion, ESA SP-365, Oct. 2000.

[16]Task 27A Completion Report, NASA Contract NAS3-99151, SPI Subcontract 97-1088-02, "Acquire TM Data for Type A and Type B Sensors for Express-A No3 Satellite (Period of 24 June 2000 to and including 30 September 2000)," M. F. Reshetnyov Science and Production Association of Applied Mechanics-Razvitie, June 2001.

[17]Task 27B Completion Report, NASA Contract NAS3-99151, SPI Subcontract 97-1088-02, "Acquire TM Data for Type A and Type B Sensors for Express-A No3 Satellite (Period of 01 October 2000 to and including 31 December 2000)," M. F. Reshetnyov Science and Production Association of Applied Mechanics-Razvitie, June 2001.

[18]Pullins, S., Dressler, R. A., Chiu, Y., and Levandier, D. J., "Ion Dynamics in Hall Effect and Ion Thrusters: $Xe^+ + Xe$ Symmetric Charge Transfer," AIAA Paper 2000-0603, Jan. 2000.

[19]Mikellides, I. G., Jongeward, G. A., Katz, I., Gardner, B. M., Mandell, M. J., and Davis, V. A., "A Hall-Effect Thruster Plume and Spacecraft Interactions Modeling Package," International Electric Propulsion Conf., IEPC Paper 2001-251, Oct. 2001.

[20]Jongeward, G. A., Katz, I., and Mikellides, I. G., "High Voltage Solar Arrays for a Direct Drive Hall Effect Propulsion System," International Electric Propulsion Conf., IEPC Paper 2001-327, Oct. 2001.

I. D. Boyd
Associate Editor